Journal of Catalysis 276 (2010) 170–180

Contents lists available at ScienceDirect

Journal of Catalysis

journal homepage: www.elsevier.com/locate/jcat

Mesoporous mordenites obtained by sequential acid and alkaline treatments – Catalysts for cumene production with enhanced accessibility

Adri N.C. van Laak, Sophia L. Sagala, Jovana Zečević, Heiner Friedrich, Petra E. de Jongh, Krijn P. de Jong *

Inorganic Chemistry and Catalysis, Debye Institute for Nanomaterials Science, Utrecht University, Netherlands

ARTICLE INFO

Article history:
Received 2 July 2010
Revised 6 September 2010
Accepted 10 September 2010
Available online 16 October 2010

Keywords:
Mordenite
Mesoporosity
Dealumination
Desilication
Alkylation
Catalysis
Cumene

ABSTRACT

Two commercially available mordenites, obtained from Zeolyst (Si/Al = 10 at/at) and BASF (Si/Al = 8 at/at), were subjected to post-synthesis treatments. The impact of acid treatment, alkaline treatment (desilication) and a combination of both on porosity, crystallinity and catalysis were studied in detail. It was found that sequential acid and alkaline treatments were most effective to obtain mesoporous mordenite with external surface areas up to 250 $m^2 g^{-1}$. Electron tomography was used to visualize the mesoporosity of a series of sequential acid- and alkaline-treated mordenite samples. Mesopore formation started close to the external surface area and progressed toward the center of the crystallites for higher porosities. Liquid-phase alkylation of benzene with propylene to cumene was chosen to study the catalytic performance of the enhanced accessibility of various mordenite samples. The activity of the most porous mordenite was found to be close to that of a commercial zeolite beta, while selectivity toward the undesired *n*-propylbenzene was found to be significantly lower for mordenite (~70 ppm) than for zeolite beta (~175 ppm). These catalytic data indicate that the acid- plus alkaline-treated mordenite could be a viable catalyst in the cumene process.

1. Introduction

Alkylation of benzene with propene to form isopropylbenzene (cumene) is an important industrial process with an annual production of 8 million tonnes [1]. Cumene is primarily used as feedstock for the co-production of phenol and acetone. Until the mid-nineties, cumene was produced with solid phosphoric acid (SPA) or $AlCl_3$ as catalysts. Because of superior selectivities and environmental benefits, the first cumene plants based on zeolite catalysts started to operate in 1996 [2]. Due to the size of the cumene molecule, 12-ring zeolites were found to be the most promising, including ultrastable Y (USY/FAU), mordenite (MOR), zeolite beta (BEA), MCM-22 (MWW) and ZSM-12 (MTW) [1], although the 10-ring zeolite ZSM-5 was found to be promising as well [3]. Because of slow diffusion in the micropores [4], it was found that zeolites with a small diffusion pathlength such as MCM-22 and zeolite beta were most active. In the MCM-22 process (Mobil–Raytheon), alkylation is believed to take place in cups located on the outer surface of the crystallites [5], thereby avoiding diffusion limitations. The high activity of zeolite beta (UOP, Q-Max™ process) is the result of nano-crystallites [6] and an efficient three-dimensional micropore system that consists of two inter-connecting 12-ring channels [7].

Typical byproducts in the cumene synthesis [8] are diisopropylbenzene (DIPB), triisopropylbenzene (TIPB), propene oligomers and *n*-propylbenzene (NPB). DIPB is converted into cumene in a subsequent transalkylation step, whereas TIPB and oligomers are considered waste. NPB formation [9,10] has to be prevented because in the downstream phenol production propionaldehyde is formed, which is an acetone contaminant. In 1996, the specification for NPB was 300 ppm [2], the Q-Max™ process claims to operate at lower than 250 ppm [11] (alkylation + transalkylation). It was found that of zeolites mentioned above, mordenite had the lowest production of *n*-propylbenzene [12,13], and from this perspective mordenite could be a very attractive catalyst.

The micropore system of mordenite consists of two pore types: 12-ring channels in the *c*-axis direction (6.7 × 7.0 Å) and 8-ring channels along the direction of the *b*-axis (3.4 × 4.8 Å) that are inaccessible above C_3-molecules [14]. Since the 8-ring channels do not inter-connect the 12-ring channels, mordenite is considered a one-dimensional zeolite. So far, there is no synthesis route for nano-crystalline mordenite available although thin needles (60 nm width) can be produced [15,16]. Commercially available mordenite crystallites have typical dimensions between 100 and 200 nm and typically form larger particles. Post-synthesis treatments with steam and acid have been described in detail in the literature. The mesoporosity after these treatment was reported as limited [17–22]. DOW reported that by cyclic dealumination, a highly active pseudo three-dimensional mesoporous mordenite (3DDM) was obtained, which was commercially applied as an

* Corresponding author. Fax: +31 30 251 1027.
E-mail address: k.p.dejong@uu.nl (K.P. de Jong).

0021-9517/$ - see front matter © 2010 Elsevier Inc. All rights reserved.
doi:10.1016/j.jcat.2010.09.011

add-on transalkylation catalyst in the cumene production [23–25]. In a study by Van Donk et al., the formation of mesopores upon acid treatment was visualized with electron tomography [26,27].

Alkaline treatment or desilication [28–31] with NaOH can be a very effective post-synthesis treatment to improve the porosity of zeolites. During contact with the alkaline solution, silicon is extracted from the framework resulting in mesoporous zeolites. Successful alkaline treatment depends on the silicon to aluminum ratio of the zeolite. If the Si/Al ratio is too low, no mesopores are formed, and when it is too high complete dissolution occurs. The optimal Si/Al ratio for alkaline treatment was found to be between 25 and 50 at/at [30]. It was shown that direct alkaline treatment on as-synthesized mordenite crystals in this optimal range indeed resulted in the formation of mesopores [32]. Bokhoven et al. [33] showed that acid treatment can be used to boost the Si/Al ratio of mordenite into this optimal range, leading to mesopore formation upon successive alkaline treatment. The crystallites used in both studies however, are up to two orders of magnitude larger than those prevailing in commercially available mordenite samples. It was shown by van Laak et al. [34] that alkaline treatment on commercially available mordenite with Si/Al ratios as low as 10 at/at can result in the formation of intra-crystalline mesopores.

In this paper, we discuss the effects of sequential acid and alkaline treatments on the structural and catalytic properties of mordenite. Initial results were acquired on a readily available commercial mordenite obtained from Zeolyst International (CBV 21A). The sequential treatments resulted in the formation of mesoporous mordenite, although the Zeolyst mordenite was found to have a limited thermal stability. Hence, the procedure as described is also applied to a more stable second zeolite sample obtained from BASF. A comprehensive study was made on post-synthesis treatments on the BASF mordenite porosity including imaging by electron tomography. Although we realize that the changes in porosity can affect the acidity of the mordenite to some extent, we have not extensively studied the latter parameter. The catalytic properties of the treated BASF mordenite samples were tested for the liquid-phase production of cumene and are compared to an industrial catalyst based on zeolite beta.

2. Experimental

2.1. Sample preparation

Mordenite samples were provided by Zeolyst International (CBV 21A) and BASF (formerly Engelhard). Zeolyst CBV 21A was delivered in NH_4 form with a Si/Al ratio of 10 at/at, BASF mordenite in sodium form with Si/Al ratio of 8 at/at. Two zeolite beta samples were supplied by Zeolyst International. The first sample, CP814 N CY (Si/Al ratio at/at 9), was an extrudate (20 wt.% SiO_2) in proton form. The second sample, CP814E (Si/Al ratio of 12.5), was supplied in NH_4 form.

As-received Zeolyst mordenite, referred to as NH_4-Zeolyst-*parent*, was converted from the ammonia form to the proton form by calcination at 773 K for 3 h using a heating rate of 1 K min^{-1}; the obtained sample will be referred to as H-Zeolyst-*parent*. As-received BASF mordenite, referred to as Na-BASF-*parent*, was ion exchanged three times under stirring in an aqueous 1 M NH_4NO_3 (p.a. Acros) solution at 353 K for 24 h, followed by filtering and washing. Per gram of mordenite 12 ml of ammonia nitrate solution was used. The ion exchanged NH_4-BASF-*parent* was calcined as described above: the obtained sample will be referred to as H-BASF-*parent*.

Acid treatment was performed by adding 10 g of H-Mordenite-*parent* in 100 ml of 3 M nitric acid (65% p.a. Acros) solution at reflux conditions for 1 h, while stirring. This was followed by filtering and washing with hot demineralized water until the pH is the filtrate was ~4. The obtained mordenite is called H-Mordenite-*acid*, subsequent calcination as described above resulted in H-Mordenite-*acid-c*.

Alkaline treatment on Zeolyst samples was performed by adding 0.7 g mordenite in 40 ml pre-heated alkaline solution (0.05–1 M NaOH) (p.a. Merck) or 1 M NH_4OH (p.a. Acros) at 343 K, while stirring. This was followed by centrifugation (Eppendorf centrifuge 5804, 5000 rpm) and decantation of the liquid followed by re-suspension with hot demineralized water. This procedure was repeated until the pH was ~7. Conversion to proton form was performed as described above. BASF samples were treated similarly; the centrifugation step was carried out at 18.000 rpm using a SS34 rotor on a Sorvall *RC5*$^+$ ultracentrifuge for 1 min. Conversion to proton form was performed as described above with 1 M NH_4NO_3, followed by calcination at 723 K. Alkaline-treated samples are indicated with *-at* added to the name. One combined acid and alkaline-treated sample was subsequently treated in 0.1 M HNO_3 solution at 323 K for 15 min. The flow diagram for the separate synthesis steps including sample designations for the as-received mordenite parent to the sequential acid/alkaline/acid-treated mordenite is represented in Scheme 1.

2.2. Structural characterization

Powder X-ray diffraction (XRD) patterns were obtained using a Bruker-Axs D8 series 2 with a $Co_{\alpha 1,2}$ source (λ = 0.179 nm). *In situ* XRD during calcination was performed in 20% O_2 in N_2 (heating with 1 K min^{-1} to 393 K for 3 h followed by heating with 1 K min^{-1} to 773 K for 3 h). Crystallinity was determined according to O'Donovan et al [20] by the summed up intensities of the (3 3 0), (1 5 0), (2 0 2), (3 5 0) and (5 1 1) reflections. The parent mordenite was assigned a crystallinity of 100%.

The porosity of the samples was studied using N_2-physisorption isotherms, which were recorded using a Micromeritics Tristar 3000 at 77 K. Prior to the physisorption measurements, the mordenite samples were dried overnight at 573 K in flowing nitrogen. The *t*-plot method was applied to obtain the micropore volume and external surface area. Pore size distributions were obtained from the adsorption branch using the BJH method. The mesopore volume was calculated by integrating these plots from 2 to 50 nm. Pore size distributions are plotted from 2 to 100 nm. Although pore sizes >50 nm are less reliable, they are still indicative of the volume of small macro-pores in the sample.

Morphology and crystal sizes were determined with a Tecnai FEI XL 30SFEG Scanning Electron Microscope (SEM) at 15 kV and with a Tecnai 20 Transmission Electron Microscope operated at 200 kV. Samples for electron tomography (ET) were prepared in

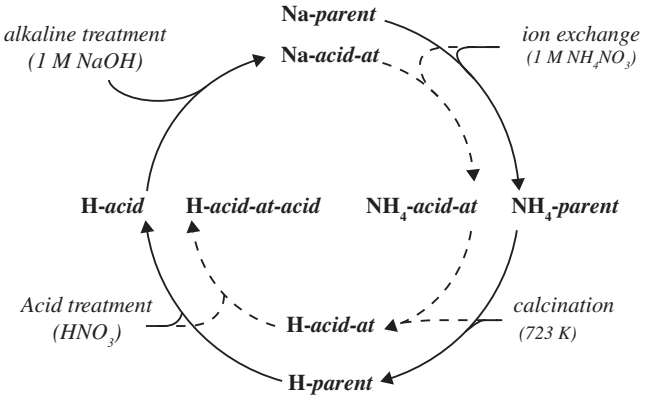

Scheme 1. Flowdiagram synthesis steps.

two steps. First, colloidal gold particles of 10 nm in size were deposited from suspension on a carbon support film on a standard Cu parallel-bar TEM grid, followed by drying in air. The carbon support film consisted of a <20-nm-thick Quantifoil R2/1 carbon film with a ~3-nm-thin continuous carbon layer on top (Quantifoil Microtools GmbH, Jena, Germany). Second, a few drops of a dilute suspension of mordenite crystals in ethanol were applied to the grid, again followed by drying in air. Tilt-series data were collected on a Tecnai 20 transmission electron microscope, which was equipped with a LaB6 electron gun (200 keV) and a TWIN objective lens. Tilt-series were recorded in bright-field TEM mode on a 2 k × 2 k CCD camera (TVIPS GmbH, Gauting, Germany) over an angular range of −75° to +75° at 1° or 2° increments. The nominal defocus was set to −600 nm (14.5 k×) and −500 nm (19 k×). Alignment of the datasets (using the 10 nm colloidal gold particles as fiducial markers) and reconstruction (by weighted backprojection) was performed in IMOD [35]. Prior to reconstruction, the aligned tilt-series was binned by a factor of 2 resulting in a final pixel size of 1.1 nm (14.5 k×) or 0.82 nm (19 k×).

Analysis of the pore network was carried out by manual segmentation in Amira (Visage Imaging, Inc.) and automated segmentation in Matlab (The Mathworks) using in part functions of the TOM toolbox [36] and the Delft image processing library (http://www.diplib.org). Segmentation in Matlab proceeded via the following: (1) median filtering of the reconstruction; (2) thresholding using the isodata algorithm [37]; (3) binary erosion; (4) selection of the largest connected object; (5) binary dilation; and (6) binary closing. Following this automated segmentation procedure, pores of at least 4 pixel in diameter, e.g. ~2.5 nm at a magnification of 19 k×, could be detected. The results of the reconstruction, manual and automated segmentation were visualized by numerical cross-sections using Amira, Matlab or IMOD.

^{27}Al MAS NMR experiments were carried out with a Bruker Avance 700 NMR spectrometer using a 2.5-mm double-resonance probe head. The resonance frequency for ^{27}Al was 182.4 MHz, and the pulse length was 6 μs. All the spectra were obtained at a spinning speed of 15 kHz, and scans were added with a recycle delay of 1 s. The ^{27}Al chemical shifts were referenced to $(NH_4)Al(SO_4)_2{\cdot}12H_2O$.

Ammonia temperature-programmed desorption (TPD) was performed with a Micromeritics Autochem II. About ~150 mg of sample was dried at 573 K. After saturating the sample at 473 K with ammonia, a 30-min dwell time was applied. Subsequently, TPD was measured while the temperature was increased to 923 K with a heating rate of 10 K min^{-1} and kept constant for 30 min.

2.3. Catalytic measurements

Catalytic tests were carried out in an autoclave stirred at 400 rpm. Benzene and propylene were tapped from industrial streams (99% plus) supplied by Dow Terneuzen, The Netherlands. For the alkylation, approximately 0.75 g of catalyst powder (sieve fraction 425–800 μm) and 270 g of benzene were loaded into a nitrogen-purged 1-l autoclave. After raising the temperature to 423 K, approximately 38 g of propylene was fed to the reactor resulting in a benzene to propylene molar ratio ~4. The reactor was then pressurized to ~40 bars by feeding nitrogen. During the reaction, samples were withdrawn from the reactor and analyzed by GC. A similar catalytic setup was used by Bellussi et al. [38].

3. Results and discussion

In Fig. 1, SEM images are shown from mordenite samples from Zeolyst and BASF as well as zeolite beta (Zeolyst CP 814E). Both mordenite samples contain small crystallites of 100–200 nm that have agglomerated into larger particles. The BASF mordenite contains also larger crystallites up to 500 nm in length. The Zeolyst material was chosen as the starting material for post-synthesis treatments because of its more homogenous morphology compared to the BASF mordenite. Zeolite beta (Fig. 1C) consists of nano-crystallites with sizes between 15 and 20 nm, which are clustered into agglomerates of about 60–100 nm, which then form larger particles up to several micrometer.

3.1. Mordenite: Zeolyst

3.1.1. Acid treatment

NH_4-Zeolyst-*parent* was calcined to obtain H-Zeolyst-*parent* that was subsequently acid treated in 3 M HNO_3 for 1 h, thereby increasing the Si/Al ratio from 10 to 30 at/at (H-Zeolyst-*acid*). With nitrogen physisorption, it was determined that the porosity did not change significantly upon acid treatment (Table 1). The crystallinity was preserved even though about three quarters of the total aluminum content of the parent mordenite was removed. This illustrates the validity of acid treatment as a tool to modify the Si/Al ratio of mordenite. However, after subsequent calcination at 773 K the crystallinity decreased to ~50% when compared to the H-Zeolyst-*acid* sample. Despite the decrease in crystallinity after calcination, no significant change on the porosity of mordenite was observed. Apparently small changes in the framework are made during calcination that are affecting the crystallinity of the mordenite, without altering the microporosity. *In situ* XRD measurements were performed to study at which temperatures the decrease in crystallinity occurs. Calcination of the as-received NH_4-Zeolyst-*parent* (Fig. 2) resulted in a small decrease in crystallinity that started around 623 K and ended when 773 K was reached. Upon calcination of the H-Zeolyst-*acid* sample, a fast decrease for all peaks was observed above 573 K (Fig. 3). If we define the crystallinity of H-Zeolyst-*parent* as 100% a decrease to ~50% is observed upon calcination of the H-Zeolyst-*acid* sample. The most likely explanation is that extra-framework aluminum (efAl) species are formed during calcination [39–41], which remain close to the

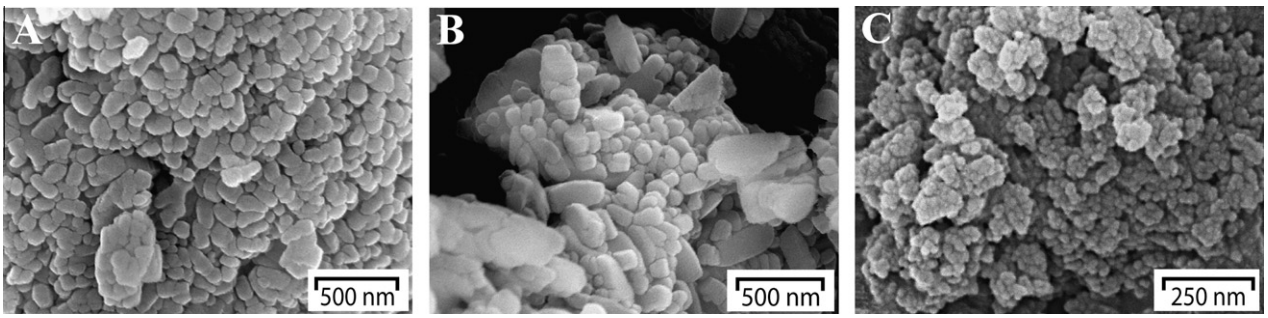

Fig. 1. SEM image (A) NH_4-Zeolyst-*parent* (mordenite), (B) Na-BASF-*parent* (mordenite) and (C) NH_4-Zeolyst CP 814E (zeolite beta).

Table 1
Textural properties and crystallinities of mordenite samples (Zeolyst).

	V_{micro}[a] ($cm^3\ g^{-1}$)	A_{ext}[a] ($m^2\ g^{-1}$)	V_{meso}[b] ($cm^3\ g^{-1}$)	V_{total}[c] ($cm^3\ g^{-1}$)	Si/Al[d] (at/at)	Crystallinities (%)
NH_4-Zeolyst-*parent*	**0.17**	**45**	**0.04**	**0.25**	10	104
H-Zeolyst-*parent*	0.20	52	0.05	0.29	10	100
H-Zeolyst-*acid*	0.19	59	0.05	0.33	30	97
H-Zeolyst-*acid-c*	0.20	57	0.05	0.33	30	49
Na-Zeolyst-*acid-at(0.05 M NaOH 60′)*	0.18	83	0.08	0.35	20	97
Na-Zeolyst-*acid-at(0.1 M NaOH 30′)*	0.17	160	0.13	0.41	17	81
Na-Zeolyst-*acid-at(0.2 M NaOH 5′)*	0.13	285	0.24	0.54	12	53
Na-Zeolyst-*acid-c-at(0.1 M NaOH 30′)*	0.18	78	0.07	0.33	20	105
Na-Zeolyst-*acid-c-at(0.2 M NaOH 5′)*	0.18	145	0.11	0.38	17	82

[a] *t*-Plot method.
[b] BJH method (adsorption branch).
[c] @ $p/p_o = 0.995$.
[d] ICP-AES.

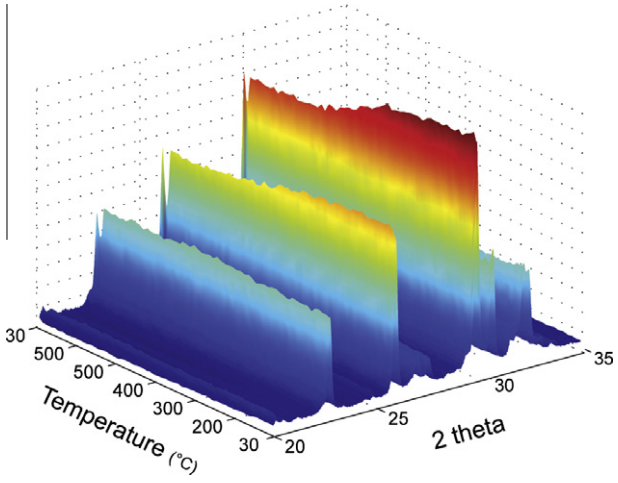

Fig. 2. *In situ* XRD: NH_4-Zeolyst-*parent*.

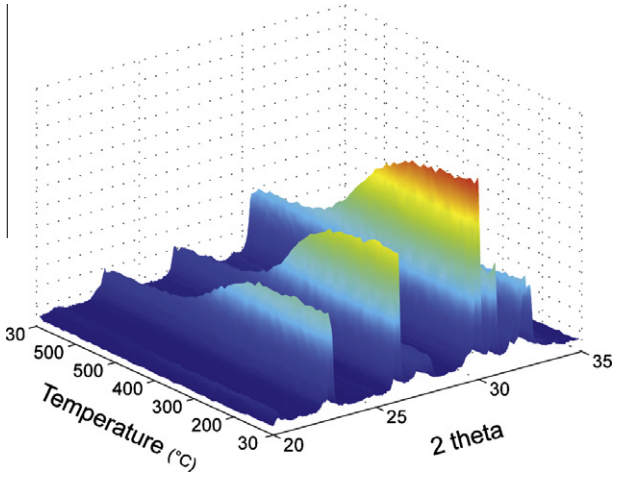

Fig. 3. *In situ* XRD: H-Zeolyst-*acid*.

extraction site as the microporosity is not affected by calcination (Table 1). From an extensive study by Katada et al. [39,40], it was concluded that extra-framework aluminum in mordenite (Tosoh, Si/Al ratio 7.5) is formed at calcination temperatures above 673 by trace amounts of water. Muller et al. [41] however, observed large differences in efAl formation for different mordenite samples. ^{27}Al MAS NMR (Fig. S1) confirmed that upon calcination of the acid-treated mordenite, additional efAl is created, and NH_3 TPD measurements (Fig. S2) show that the calcination results in a decrease in the Brønsted acid sites by ~50%.

For the Zeolyst mordenite, we can conclude that acid treatment is a powerful technique to increase the Si/Al ratio. Subsequent calcination at 773 K however, leads to the loss of crystallinity and Brønsted acid sites and to the formation of efAl. These changes most likely take place on a very local scale because the microporosity is unaffected.

3.1.2. Acid + alkaline treatment

Alkaline treatment was performed on the H-Zeolyst-*acid* sample in 0.05 M NaOH for 60 min, 0.1 M NaOH for 30 min and in 0.2 M NaOH for 5 min at 343 K. These conditions are slightly milder than those reported in the literature [32] because of the smaller crystallite sizes (~150 nm vs. 10 μm). From nitrogen physisorption data (Table 1, Fig. S3), we can conclude that all three experiments led to an increased porosity. The effect of the mild alkaline treatment in 0.05 M NaOH was limited, but treatment in 0.1 M for 30 min resulted in mordenite with an external surface area of 160 $m^2\ g^{-1}$ and a slight decrease in crystallinity from 97% to 81%. Treatment in 0.2 M NaOH resulted in an external surface area of 285 $m^2\ g^{-1}$ and a mesopore volume of 0.26 ml g^{-1}. The BJH pore size distribution (Fig. S3-B) of the Na-Zeolyst-*acid-at(0.2 M NaOH 5′)* sample shows a large volume of mesopores below 10 nm in size. A TEM image (Fig. 4) visualizes the mesopores as interruptions of the lattice planes, with dimensions between 4 and 8 nm. A decrease in micropore volume (0.20–0.13 $cm^3\ g^{-1}$) was observed, which can possibly be attributed to the external surface area effect as described by Camblor et al. [6]. Besides the decrease in

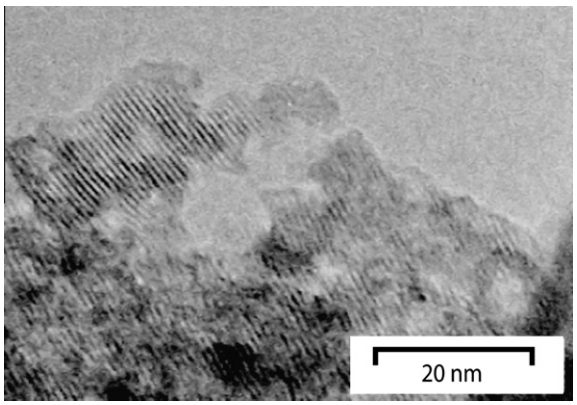

Fig. 4. TEM image Na-Zeolyst-*acid-at(0.2 M NaOH 5′)*.

micropore volume, there was also a significant decrease in crystallinity observed from 97% for the H-Zeolyst-*acid* to 53% for Na-Zeolyst-*acid-at(0.2 M NaOH 5′)*.

Similar experiments with 0.1 and 0.2 M NaOH were performed on the acid-treated mordenite after calcination, H-Zeolyst-*acid-c*. Again for both samples, an increase in porosity was observed although the volume of mesopores was considerably lower than for non-calcined sample (Table 1, Fig. S4). The 0.1 M NaOH and 0.2 M NaOH treatments resulted in external surface areas of 78 $m^2 g^{-1}$ and 145 $m^2 g^{-1}$, respectively, compared to 160 $m^2 g^{-1}$ and 285 $m^2 g^{-1}$ for the non-calcined samples. The crystallinity after treatment in 0.1 M NaOH was restored from 50% to 105% and to 82% after the 0.2 M NaOH treatment. The low mesoporosity that was obtained after 0.1 M NaOH treatment suggests that dissolution of amorphous material to increase the crystallinity is unlikely. More likely is that local defects close to the extraction site are the reason for the loss of crystallinity and possibly that re-insertion of aluminum species into the zeolite framework occurs during alkaline treatment, thereby restoring crystallinity. Similar results were described by Groen et al. [31] for ZSM-5 in which a steam treatment at 873 K followed by alkaline treatment resulted in lower mesoporosity compared to an alkaline treatment only. The pore size distribution of the combined acid- and alkaline-treated samples (Figs. S3-B and S4-B) show a comparable pattern for all samples, only the volume of mesopores varies.

A lower NaOH concentration leads to a lower degree of porosity, which could be related to a penetration gradient inside the particle or within the crystallite. The main difference between the non-calcined and the calcined samples is the nature of the aluminum species. The difference in porosity after identical alkaline treatment on non-calcined and calcined samples hence indicates that the nature of the aluminum species influence the alkaline treatment greatly. The different aluminum species before and after calcination are located within the micropores, and hence the differences in porosity are expected within the crystallites rather than within the particles. In summary, we can conclude that highly porous mordenite can be obtained by sequential treatment acid and alkaline treatment on Zeolyst CBV 21A mordenite. The stability after post-synthesis treatments however, is considered poor, and therefore a second mordenite supplied by BASF was studied.

3.2. Mordenite: BASF

3.2.1. BASF: acid treatment

Na-BASF-*parent* was ion exchanged with 1 M NH_4NO_3 followed by calcination to obtain H-BASF-*parent* that was subsequently stirred in 3 M HNO_3 at reflux conditions for 1 h, resulting in a dealuminated mordenite with Si/Al ratio 22 (H-BASF-*acid(22)*). TEM/EDX measurements (Fig. S5) were performed on large and small crystallites that indicated the presence of local Si/Al ratio variations between 16 and 23 at/at. As both these values are below the optimum Si/Al ratio for successful desilication [30], a second batch of acid-treated mordenite was prepared. Acid treatment was similar as for the H-BASF-*acid(22)* sample with a longer reflux time of 1.5 h, resulting in a Si/Al ratio of 30 (H-BASF-*acid(30)*). From nitrogen physisorption, listed in Table 2, it was determined that the porosity of the mordenite did not change significantly (Fig. 5), though a small increase in external surface area of ~20 m^2 was observed. After acid treatment only we observed that crystallinity was retained, which decreased upon calcination to 72%. These results are in line with the results obtained for the Zeolyst mordenite, although the thermal stability of the acid-treated BASF mordenite is superior to that of the acid-treated Zeolyst mordenite.

3.2.2. BASF: alkaline treatment

In the literature, it is shown [34] that direct alkaline treatment on the Na-BASF-*parent* mordenite in 1 M NaOH solution at 343 K for 15 min resulted in the formation of mesopores. When these conditions were applied, silicon and aluminum were dissolved, though silicon was dissolved in slightly larger amounts thereby decreasing the bulk Si/Al ratio in the alkaline-treated BASF mordenite. The alkaline treatment experiments were repeated with increased treatment time of 20 min resulting in an increase in the external surface area to 128 $m^2 g^{-1}$ compared to 43 $m^2 g^{-1}$ for the H-BASF-parent and a decrease in Si/Al ratio from 9 to 7 at/at (Table 2). From the BJH pore size distributions (Fig. 5B), we can conclude that after alkaline treatment and subsequent ion exchange and calcination (H-BASF-at) a wide range of meso- and macro-pores were obtained.

Table 2
Textural properties and crystallinities of mordenite samples (BASF) and zeolite beta (Zeolyst).

	V_{micro}[a] ($cm^3 g^{-1}$)	A_{ext}[a] ($m^2 g^{-1}$)	V_{meso}[b] ($cm^3 g^{-1}$)	V_{total}[c] ($cm^3 g^{-1}$)	Si/Al[d] (at/at)	Crystallinities (%)
Na-BASF-*parent*	0.17	36	0.03	0.26	9	102
H-BASF-*parent*	0.19	43	0.04	0.30	9	100
H-BASF-*at*	0.17	128	0.17	0.57	7	91
H-BASF-*acid(22)-c*	0.19	67	0.05	0.31	22	82
H-BASF-*acid(22)-c-at(NaOH)*	0.17	170	0.20	0.54	13	83
H-BASF-*acid(22)-c-at(NH_4OH)*	0.19	94	0.08	0.36	19	90
H-BASF-*acid(30)*	0.19	59	0.05	0.30	30	93
H-BASF-*acid(30)-c*	0.20	61	0.05	0.30	30	72
Na-BASF-*acid(30)-at(NaOH)*	0.15	289	0.30	0.71	–	89
NH_4-BASF-*acid(30)-at(NaOH)*	0.16	235	0.30	0.68	–	94
H-BASF-*acid(30)-at(NaOH)*	0.16	248	0.33	0.74	–	81
H-BASF-*acid(30)-at(NaOH)-acid*	0.16	250	0.33	0.78	22	89
H-Beta Zeolyst CP814 N CY[e,f]	0.17	225	0.38	0.81	9	–
NH_4-Beta CP 814E	0.18	230	0.36	0.83	12.5	–
H-Beta CP 814E	0.17	227	0.36	0.83	12.5	–

[a] *t*-Plot method.
[b] BJH method (adsorption branch).
[c] @ $p/p_o = 0.995$.
[d] ICP-AES.
[e] Extrudate 20 wt.% SiO_2.
[f] Data based on pure zeolite beta.

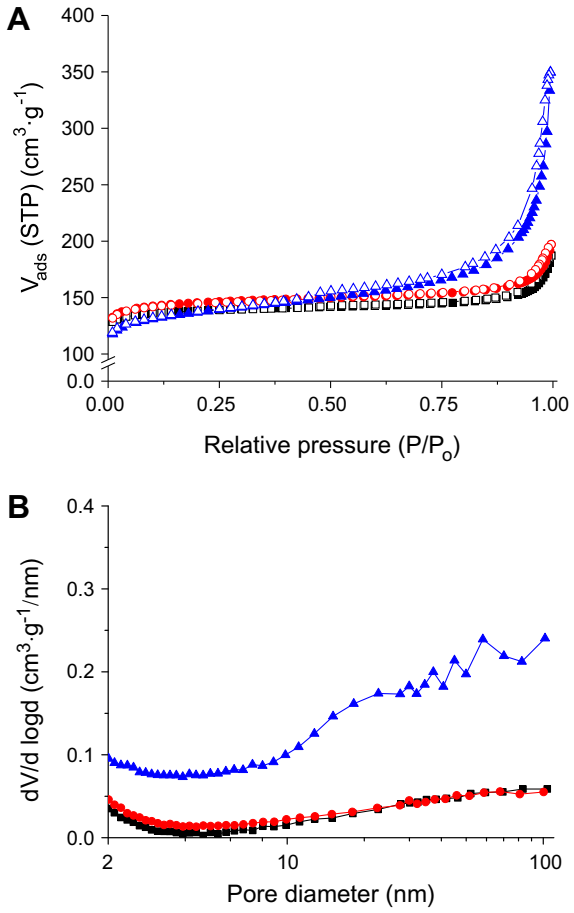

Fig. 5. (A) N_2 adsorption (solid symbols) and desorption (open symbols); and (B) BJH pore size distribution: ■ H-BASF-*parent*, ● H-BASF-*acid(22)-c* and ▲ H-BASF-*at*.

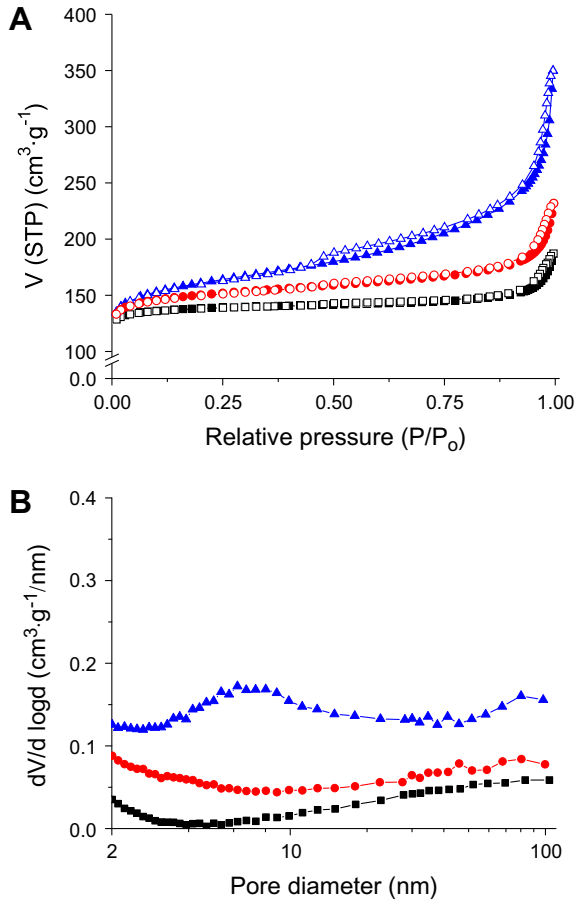

Fig. 6. (A) N_2 adsorption (solid symbols) and desorption (open symbols); and (B) BJH pore size distribution: ■ BASF H-parent, ● H-*BASF-acid(22)-c-at(NH_4OH)* and ▲ H-BASF-*acid(22)-c-at*(NaOH).

3.2.3. BASF: acid + alkaline treatment

Alkaline treatment was performed on the H-BASF-*acid(22)-c* in a 0.2 M NaOH solution at 343 K for 8 min, followed by ion exchange and calcination. This resulted in mesoporous mordenite with an external surface area of 170 $m^2\,g^{-1}$ and micropore volume of 0.17 $cm^3\,g^{-1}$ (Table 2). The pore size distribution in Fig. 6B indicates that small most likely intra-crystalline mesopores are formed with a predominant size of 8 nm. Besides these small pores, there is also a significant amount of large meso- and macro-pores that show similarities with the pores created with direct alkaline treatment on the Na-BASF-*parent*. Apparently, treatment in 0.2 M NaOH at higher Si/Al ratios dissolves part of the outer layer of the crystallites, similar to the strong alkaline treatment in 1 M NaOH for lower Si/Al ratios. An alternative alkaline treatment on the H-BASF-*acid(22)-c* sample was performed with 1 M NH_4OH at 343 K. Treatment with NH_4OH has the advantage that a simple calcination would suffice to obtain the proton from, thereby avoiding additional ion exchange steps. Treatment with NH_4OH resulted in a limited increase in external surface area from 67 to 94 $m^2\,g^{-1}$ after calcination. Important is that micropore volume was preserved, and if we compare the pore size distribution of the 1 M NH_4OH treatment (Fig. 6B) with the 0.2 M NaOH treatment, we observe fewer and smaller (below 8 nm) mesopores and a significantly lower volume of large meso- and macro-pores. A third experiment was performed on the H-BASF-*acid(30)* sample that was not calcined after acid treatment. Alkaline treatment was performed with 0.2 M NaOH for 8 min at 343 K resulting in the formation of highly porous mordenite (Table 2) with an external surface area of 287 $m^2\,g^{-1}$. The micropore volume decreased from 0.20 to 0.15 $cm^3\,g^{-1}$, while the mesopore volume was increased from 0.04 to 0.30 $cm^3\,g^{-1}$. The BJH pore size distribution (Fig. S6-B) shows a similar pore size distribution as the identically treated H-BASF-*acid(22)-c-at(-NaOH)* sample, although the mesopore volume is much higher. This indicates that the small difference in Si/Al ratio after acid treatment (30 vs. 22) and calcinations after acid treatment have an influence on the mesopore volume but not on the size of pores, similar as what was observed for the Zeolyst mordenite. A difference is that the Zeolyst mordenite has smaller mesopores after acid and alkaline treatments, which could be related to the smaller crystallite size. To obtain the active catalyst, Na-BASF-*acid(30)-at(NaOH)* was ion exchanged into NH_4-BASF-*acid(30)-at (NaOH)*, which resulted in a decrease in external surface area (from 289 to 235 $m^2\,g^{-1}$) and a slight increase in micropore volume (0.15–0.16 $cm^3\,g^{-1}$). A third effect is visible in the mesopore size in which part of the 2–4 nm mesopores are converted into larger 4–10 nm mesopores (Fig. S6-B). These changes are most likely because of removal of amorphous species. Calcination was performed at 723 K, which was reported to be the lowest calcination temperature to convert NH_4 sites into H-sites [39], thereby producing as few efAl species as possible. To remove possibly formed efAl species, a mild acid treatment in 0.1 M HNO_3 at 323 K for 15 min was performed. The final product is a highly mesoporous H-mordenite with a Si/Al ratio of 22 at/at and a crystallinity of 89%, which will be referred to as H-BASF-*acid(30)-at (NaOH)-acid* (Table 2, Fig. 7).

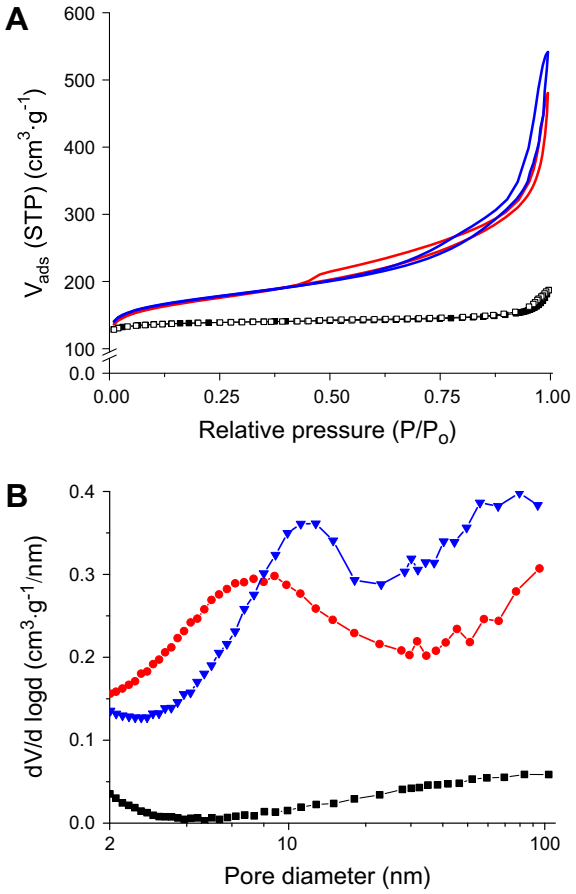

Fig. 7. (A) N_2 adsorption (solid symbols) and desorption (open symbols); and (B) BJH pore size distribution: ■ BASF H-parent (black), ● H-BASF-*acid(30)-at(NaOH)-acid* (red) and ▼ CP814E-cal (blue). (For interpretation of the references to color in this figure legend, the reader is referred to the web version of this article.)

3.3. Zeolite beta and mesoporous mordenite

Zeolite beta (CP814E) has a large external surface area of 227 $m^2\,g^{-1}$ combined with a micropore volume of 0.17 $cm^3\,g^{-1}$ (Table 2). For the CP814 N CY, the textural properties are slightly different due to the added SiO_2, but the morphology of the two zeolite beta samples is similar. If we compare zeolite beta (CP814E) with the most porous mordenite sample (H-BASF-*acid(30)-at(NaOH)-acid*), we observe similar N_2-physisorption isotherms (Fig. 7A). The differences between these the two samples becomes visible when we compare the pore size distribution (Fig. 7B), which shows a predominant mesopore size of 12 nm for the CP814E sample against 8 nm for BASF mordenite. Although the porosities of these two zeolites are similar, their origin is very different with purely inter-crystalline mesopores for the CP814E sample, while those of the mordenite are primarily intra-crystalline.

3.4. Electron tomography

The porosities of several BASF mordenite samples were further analyzed with electron tomography (ET) [42]. Low-dose TEM images were acquired to prevent degradation of the material during the tilt-series. The ET results are described according to increasing porosity (Table 2): H-BASF-*acid(22)-c-at(NH_4OH)*, H-BASF-*at*, H-BASF-*acid(22)-c-at(NaOH)* and H-BASF-*acid(30)-at(NaOH)-acid*.

In Fig. 8, a TEM image, a numerical reconstructed cross-section and a segmented cross-section of H-BASF-*acid(22)-at(NH_4OH)* through the middle of the particle are shown. We observed that small intra-crystalline mesopores are located primarily in the small crystallites and at the edges of the large crystallites. Nonetheless, most of the crystallites have a dense interior and thus no mesoporosity. In Fig. 9, similar data are shown for the H-*BASF-at* sample. The 1 M NaOH solution has dissolved part of the crystallites, thereby creating large inter-crystalline mesopores. There are also small intra-crystalline mesopores present in the small and large crystallites. These intra-crystalline mesopores are present throughout the sample even at the center of the large crystallite at the left hand side (Fig. 9C). For the combined acid- and alkaline-treated sample with sodium hydroxide, H-*BASF-acid(22)-c-at(NaOH)*, a porous structure is observed (Fig. 10). The tomography and segmented data show the existence of a large number of pores (3–8 nm) inside the crystallites. The intra-crystalline mesopores however, are primarily located in the small crystallites and close to the outer surface of the larger crystallites. In Fig. 11, the H-BASF-*acid(30)-at(NaOH)-acid* sample is depicted that indicates a highly porous material. In Fig. 11C, a manually segmented cross-section (Fig. 11A, white outline) through the agglomerate shows that a uniform distribution of the pores is present throughout the whole agglomerate. The added mesopores result in a shorter diffusion path length (half the length of the crystal) from ~70 nm for the parent to ~10 nm (Fig. 11C) for the mesoporous mordenite. Analysis of the pore sizes present in Fig. 11C (Fig. S7) resembles the BJH pore size distribution (Fig. 7) for pores of 4 nm and larger. Below 4 nm, less than expected pores are observed, which is most likely the result of the limited resolution due to the low-dose TEM experiments. This suggests that the actual porosity is most likely higher than shown in Fig. 11C. Automated segmented cross-sections visualize even less small mesopores (Fig. S8). A second isolated large particle ~300 nm (Fig. 11A, black outline) was manually segmented (Fig. S9). For this crystallite, large differences in pore sizes are observed with large intra-crystalline mesopores (up to 40 nm) present close to the outer surface, while the pores in the center are few and small. A manually analyzed tomogram (Fig. S9) shows that the majority of the mesopores are in connection with the outer surface, thereby maximizing the mass-transport through the mordenite sample.

4. Catalysis

Alkylation of benzene with propylene to form cumene was chosen as a model reaction to evaluate the effect of the post-synthesis treatments on the catalytic performance of BASF mordenite. As a reference material, zeolite beta (Zeolyst CP814 N CY) was used, which has catalytic properties close to the industrial catalyst.

The as-synthesized BASF mordenite (H-BASF-*parent*) has a low activity (Table 3) compared to zeolite beta (CP814 N CY), which is over 41 times as active. Besides a low activity H-BASF-*parent* produces a large amount of oligomers that leads to lower selectivity followed by deactivation. This is an uncharacteristic feature for mordenite in general as other mordenite samples in the literature show at least 98% selectivity [13,34] toward the desired products cumene/diisopropylbenzene (DIPB). The formation of DIPB is comparable with zeolite beta, with mordenite more selective toward the para-isomer (2.5:1 para/meta), while zeolite beta produces similar amounts (1:1 para/meta). The formation of triisopropylbenzene (TIPB) and *n*-propylbenzene (NPB) is lower for mordenite [12,13]. Upon acid treatment, a negligible increase in porosity was observed and also the catalytic activity increases only marginal (Table 3) compared to the H-BASF-*parent*. The slight increase in

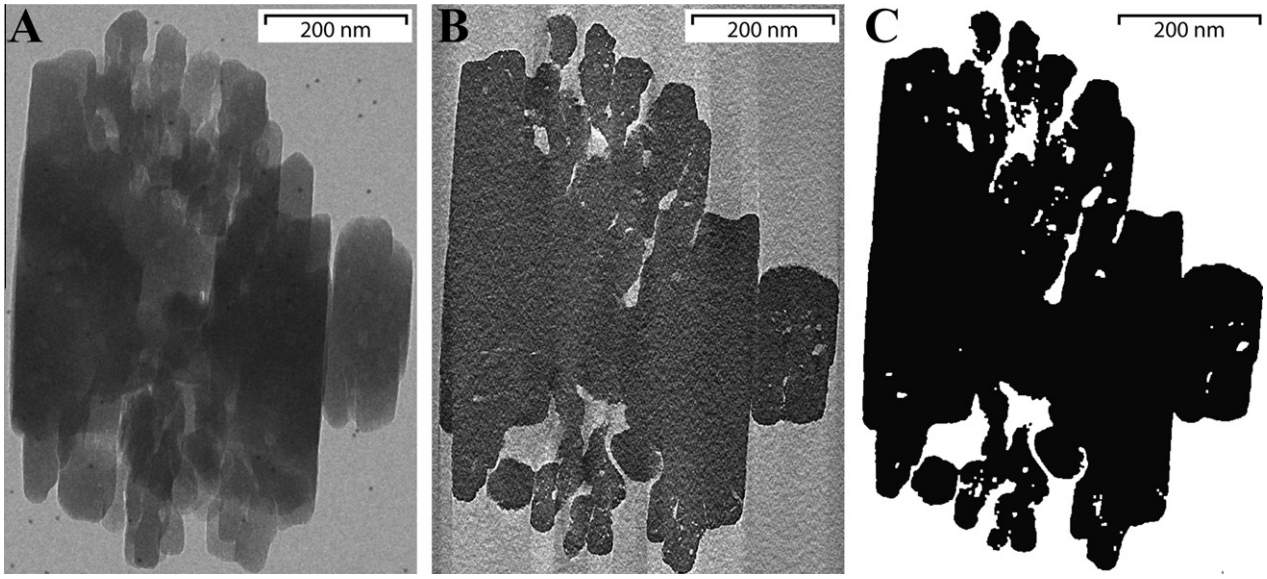

Fig. 8. H-BASF-*acid(22)-c-at(NH$_4$OH)* A_{ext} = 94 m^2 g^{-1}: (A) TEM, (B) ET reconstruction cross-section (thickness 1.1 nm) and (C) segmentation.

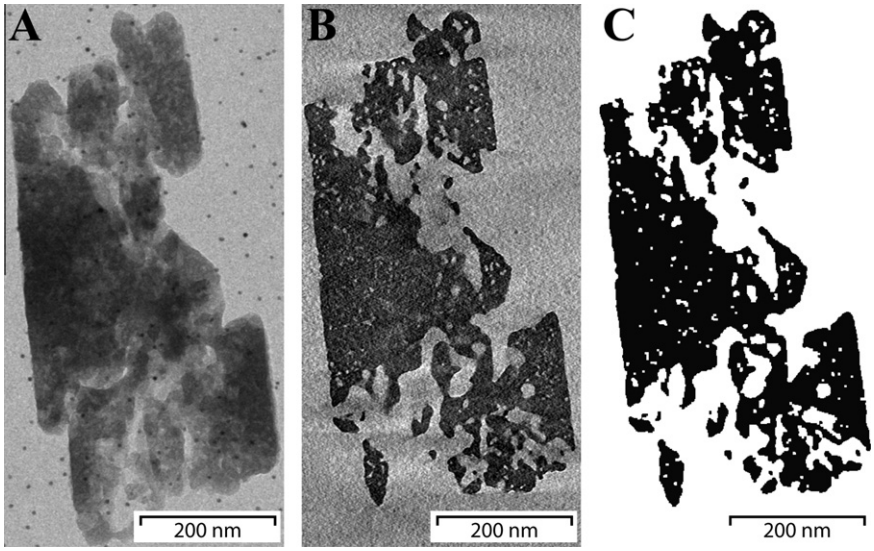

Fig. 9. H-BASF-at A_{ext} = 128 m^2 g^{-1}: (A) TEM, (B) ET reconstruction cross-section (thickness 1.1 nm) and (C) segmentation.

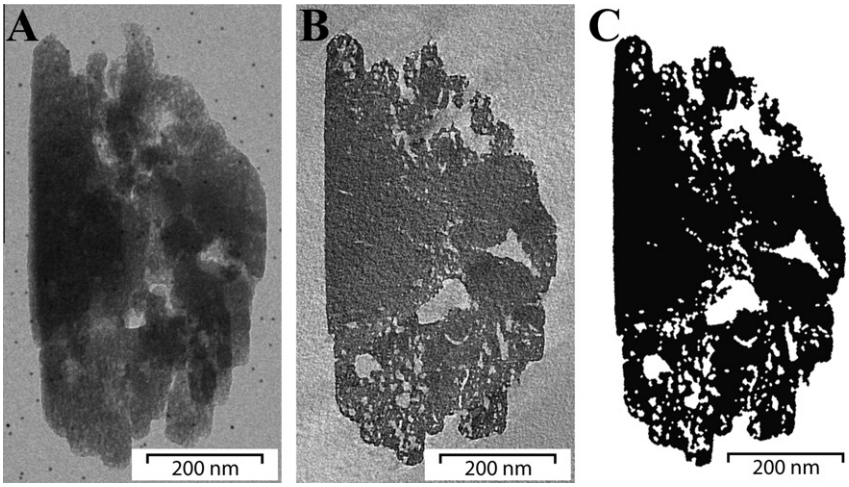

Fig. 10. H-BASF-*acid(22)-c-at(NaOH)* A_{ext} = 170 m^2 g^{-1}: (A) TEM, (B) ET reconstruction cross-section (thickness 1.1 nm) and (C) segmentation.

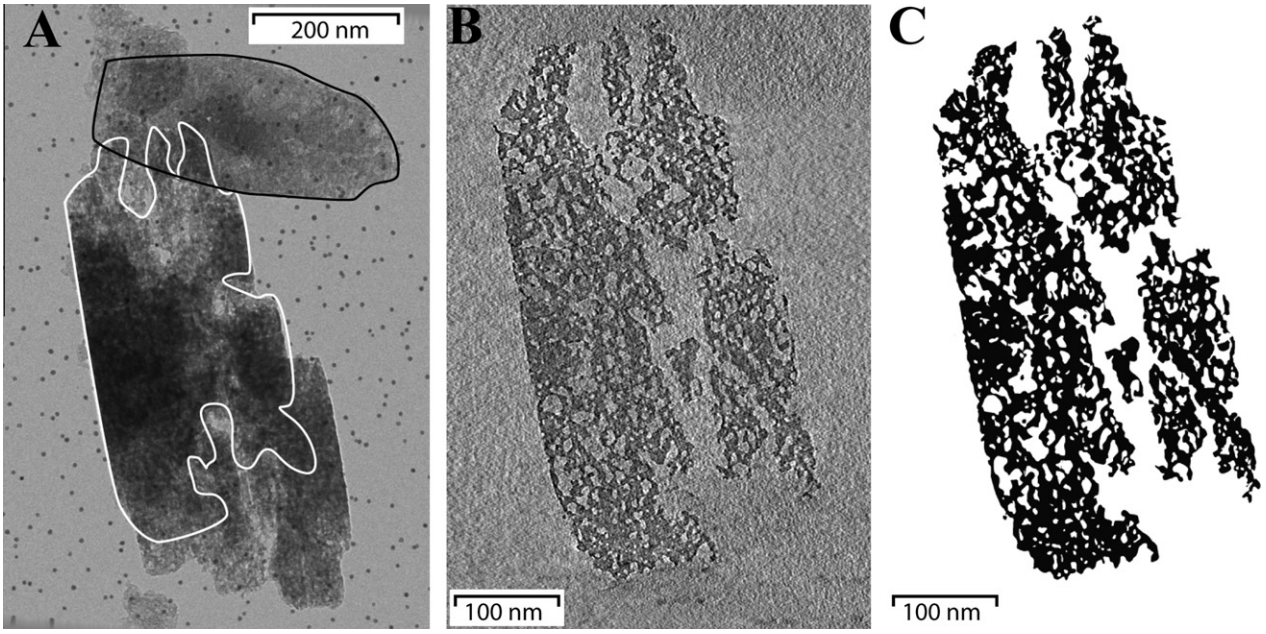

Fig. 11. H-BASF-*acid(30)-at(NaOH)-acid* A_{ext} = 250 $m^2\ g^{-1}$: (A) TEM, (B) ET reconstruction cross-section (thickness 0.8 nm) and (C) (manual) segmentation.

Table 3
Benzene alkylation with propylene; influence of post-synthesis treatments on BASF mordenite, with zeolite beta as a reference.

	H-BASF-*parent*	H-BASF-*acid(30)*	H-BASF-*at*	H-BASF-*acid(22)-c-at(NH_4OH)*	H-BASF-*acid(22)-c-at(NaOH)*	H-BASF-*acid(30)-at(NaOH)-acid*	CP814N CY[a]
Activity							
Initial rate (mol $g^{-1}\ s^{-1}$) × 10^{-3}	0.28	0.48	1.4	2.5	4.0	7.3	11
Initial rate (normalized)	1	1.6	5.4	9	15	27	41
Propene selectivity							
Cumene	75	73	79	69	72	68	84
Di-isopropylbenzene (DIPB)	15	17	20	25	23	25	15
Oligomers	10	10	1	6	5	7	1
DIPB selectivity							
Meta/para ratio	0.40	0.31	0.40	0.35	0.37	0.34	1
Side products							
Tri-isopropyl benzene (ppm)	87	–	640	370	808	700	1160
n-Propyl cumene (ppm)	77	–	82	63	71	65	175

[a] 0.80 g Zeolite beta.

activity could be the result of the increased Si/Al ratio from 8 to 30 at/at, which results in higher acid site strength [43]. The most significant change is a decrease in NPB that was below the detection limit of the GC.

The combined acid and mild alkaline treatment of H-BASF-*acid(22)-c-at(NH_4OH)* resulted in the formation of small mesopores close to the outer surface with an external surface area of 94 $m^2\ g^{-1}$ (Table 2, Fig. 8) .These intra-crystalline mesopores resulted in a nine times higher activity compared to the parent. Besides the increased activity, more DIPB and slightly less NPB was formed than for the parent. Direct alkaline treatment on the parent mordenite did result in inter- and intra-crystalline mesoporosity and a high external surface area of 128 $m^2\ g^{-1}$, and also a five times increase in catalytic activity. Interesting is that upon alkaline treatment, the production of oligomers is greatly suppressed and a 99% selectivity is obtained. These propene oligomers are possibly formed at weak acid sites located on the external surface area, at these sites the benzene to propene ratio is similar as the feed ratio, while the benzene to propene ratio on the inside of the micropore channels is, accordingly to simulations [44], expected to be significantly higher. Upon alkaline treatment in 1 M NaOH, these species might be dissolved, leaving only the highly selective Brønsted acid sites in the micropores as catalytic sites. Unexpected is that the H-BASF-*at* sample is less active compared to the H-BASF-*acid(22)-c-at(NH_4OH)* sample, despite the higher degree of porosity. After 4 h of reaction however, the higher selectivity of the H-BASF-*at* sample results in a higher conversion of propylene compared to H-BASF-*acid(22)-c-at(NH_4OH)* (Fig. S10). The higher degree of porosity of the H-BASF-*acid(22)-c-at(NAOH)* (A_{ext} = 170) results in a 15 times enhanced catalytic activity compared to the parent, and has similar selectivities as the H-BASF-*acid(22)-c-at(NH_4OH)* sample. For the most porous H-BASF-*acid(30)-at(NaOH)-acid* sample, we observed an enhanced catalytic activity of 27 times that of parent and an activity that is close to the activity of zeolite beta (Fig. 12). Selectivities for this sample are similar as for other combined acid and alkaline treatments, with a large DIPB production and oligomer formation and low NPB formation.

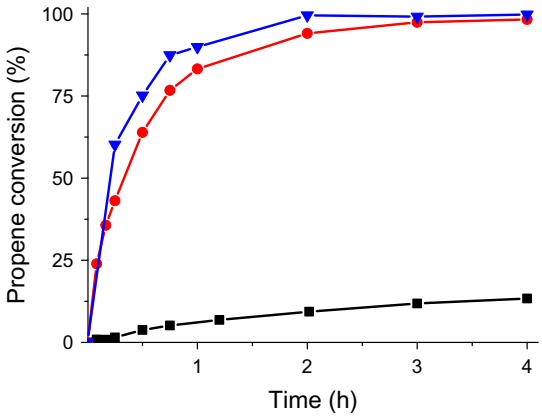

Fig. 12. Benzene alkylation with propylene: ■ BASF H-parent, ● H-BASF-*acid(30)-at(NaOH)-acid*, ▲ Zeolyst CP814E-cal (zeolite beta).

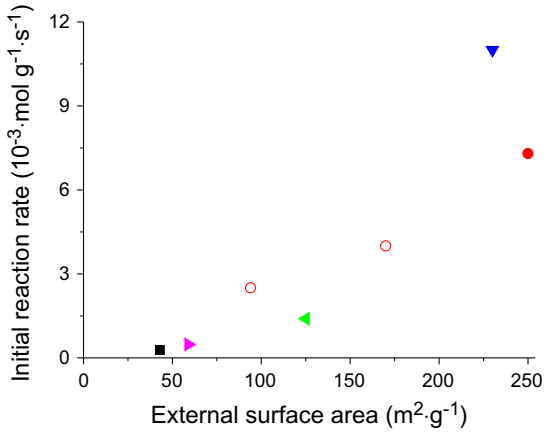

Fig. 13. Initial reaction rate vs. A_{ext} of ■ H-BASF-parent, ► H-BASF-acid, ◄ H-BASF-at, ○ H-BASF-acid(22)-c-at(NH_4OH), ⊙ H-BASF-acid(22)-c-at(NaOH), ● H-BASF-*acid(30)-at(NaOH)-acid* and ▼ zeolite Beta.

For all samples, a significantly lower NPB concentration is measured than for zeolite beta, this seems to be closely related to acid site strength. To verify this relation, the acid sites of the mordenite have to be studied in detail. This is possible by performing IR experiments with alkyl-pyridines as described by Thibault-Starzyk et al. [45]. In Fig. 13, the catalytic activity is plotted against the external surface area. For the combined- acid and alkaline-treated samples (red circles), a positive relation between external surface area and catalytic activity is observed, which confirms strong mass transfer limitations. Strong mass transfer limitation implies a Thiele Modulus (φ) larger than 2 [46]. If $\varphi > 2$, then the activity becomes proportional to the external surface area. The latter conclusion should not be confused with catalytic activity only occurring at the external surface. For $\varphi > 2$, strong internal concentration gradients exists, but still the catalysis predominantly takes place inside the micropores of the zeolite catalyst.

The activity of the direct alkaline-treated mordenite is considerably lower despite the high porosity. The largest difference between the alkaline-treated and the sequential acid- and alkaline-treated samples is the lower Si/Al ratio. This suggests that the best catalytic results with mordenite are obtained by raising both the porosity as well as the Si/Al ratio. Another effect of the added porosity might be that deactivation by pore blocking due to coke deposits [47] is expected to be lower. Despite the high porosities of the mesoporous mordenite zeolite beta is still more active. The higher activity of zeolite beta is most likely the result of the three-dimensional micropore channel system.

5. Conclusion

The effect of acid and alkaline treatment and the combination of both treatments on the porosity of mordenite was investigated on commercial mordenite samples supplied by Zeolyst and BASF. Both samples consist of small crystallites ~150 nm that have agglomerated into larger particles. It is shown that acid treatment does not lead to significant (meso) porosity; however, the Si/Al ratio can be increased significantly with preserved crystallinity and (micro) porosity. Calcination of the acid-treated mordenite however, can lead to the formation of extra-framework aluminum and loss of up to 50% of the Brønsted acid sites and crystallinity. Direct alkaline treatment in 1 M NaOH on the parent mordenite leads to an increased porosity (A_{ext}: 128 $m^2\,g^{-1}$), while at the same time the Si/Al ratio decreases from 9 to 7 at/at. Electron tomography studies indicate that large parts of the crystallites have been dissolved leading to large inter-crystalline meso- and macro-pores as well as small intra-crystalline mesopores that are present throughout the sample. If alkaline treatment is performed on an acid-treated sample, highly porous mordenite (A_{ext}: 250–300 $m^2\,g^{-1}$) can be obtained. If a calcination is performed between acid and alkaline treatment significantly lower porosities (A_{ext}: ~145 $m^2\,g^{-1}$) are obtained, which is most likely the result of efAl formed during calcination that prohibits the formation of mesopores upon alkaline treatment. A series of subsequent acid- and alkaline-treated samples were prepared with increasing porosities (A_{ext}: 95, 170 and 250 $m^2\,g^{-1}$, Si/Al ratios: 19, 13 and 22 at/at) and analyzed with electron tomography. It shows that mesopores start at the edges of the crystallites and progresses toward the centers at higher mesoporosities. For the most porous mordenite, small mesopores (3–8 nm) throughout the sample were observed, although large (up to 40 nm) intra-crystalline mesopores were present as well.

Liquid-phase alkylation of benzene with propylene to form cumene was performed to study the catalytic performance of the post-synthesis-treated mordenite samples. The parent mordenite displayed low activity as well as low selectivity toward cumene/DIPB (90%) due to propene oligomerization, where >98% selectivity is expected based on literature values [13,34]. The acid treatment did not result in a significant improvement of the catalytic performance, indicating that the Si/Al ratio is of limited influence. For the alkaline-treated samples, a five times higher catalytic activity was observed compared to the parent. Interesting is that after alkaline treatment, a >99% selectivity toward cumene/DIPB was observed, which is likely the result of dissolution of weak Lewis acid sites on the external surface of the crystallites. The series of combined acid and alkaline treatment with increasing porosity resulted in increased catalytic activity by 9, 15 and 27 times, respectively, with a positive relation between external surface area and catalytic activity. The catalytic activity of the alkaline-treated sample was significantly below the correlation obtained for the acid plus alkaline-treated samples. This could indicate that the Si/Al ratio can be an important parameter at higher porosities. Selectivity toward undesired *n*-propylbenzene was found to be decreasing with increasing Si/Al ratio, which could be the result of increased acid site strength. The activity of mesoporous mordenite (A_{ext}: 250 $m^2\,g^{-1}$, Si/Al ratio: 22 at/at) was found to be close to the activity zeolite beta (A_{ext}: 227 $m^2\,g^{-1}$, Si/Al ratio: 9 at/at), which is 41 times as active as the parent mordenite and the commercial catalyst for cumene production [1]. The selectivity toward cumene/DIPB for the mesoporous mordenite (93%) was lower compared to the zeolite beta catalyst (99%) due to the formation of propene oligomers. Formation of DIPB was also found to be higher than

for zeolite beta with primarily para DIPB formed, while selectivity toward NPB was found to be three times lower (~70 vs. 177 ppm). These results show that the acid–alkaline treatment route to obtain mesoporous mordenite can result in a viable catalyst in the cumene process as an alkylation or transalkylation catalyst. Finally, we point out that more detailed characterization, in particular of the acidic properties, is advocated for these mesoporous mordenites in order to arrive at a comprehensive understanding of their catalytic performance.

Acknowledgments

We would like to thank Dr. K.R. Bayense (BASF, Utrecht, The Netherlands) and Dr. F. Winter (Shell, Amsterdam, The Netherlands) for supplying mordenite samples, Prof. Dr. J.A. van Bokhoven and N. Danilina (ETH, Zurich) for ^{27}Al MAS NMR measurements and M.S.U. Samson, Dr. M.J. van der Aalst and Dr. G. Meima (Dow Terneuzen, The Netherlands) for catalytic tests and ACTS-ASPECT for financial support.

Appendix A. Supplementary material

Supplementary data associated with this article can be found, in the online version, at doi:10.1016/j.jcat.2010.09.011.

References

[1] C. Perego, P. Ingallina, Catal. Today 73 (2002) 3–22.
[2] G.R. Meima, M.J.M. van der Aalst, M.S.U. Samson, J.M. Garces, J.G. Lee, Erdoel, Erdgas, Kohle 112 (1996) 315–318.
[3] W.W. Kaeding, R.E. Holland, J. Catal. 109 (1988) 212–216.
[4] D.M. Ruthven, M.F.M. Post, in: H. Van Bekkum, E.M. Flanigen, P.A. Jacobs, J.C. Jansen (Eds.), Introduction to Zeolite Science and Practice, second ed., Elsevier, Amsterdam, 2001, pp. 525–577.
[5] A. Corma, V. Martínez-Soria, E. Schnoeveld, J. Catal. 192 (2000) 163–173.
[6] M.A. Camblor, A. Corma, S. Valencia, Microporous Mesoporous Mater. 25 (1998) 59–74.
[7] C. Bearlocher, L.B. McCusker, D.H. Olsen, Atlas of zeolite framework types, 2007.
[8] J. Cejka, B. Wichterlova, Catal. Rev. – Sci. Eng. 44 (2002) 375–421.
[9] B. Wichterlová, J. Cejka, N. Zilková, Microporous Mater. 6 (1996) 405–414.
[10] I. Irina Ivanova, V. Montouillout, C. Fernandez, O. Marie, J.-P. Gilson, Microporous Mesoporous Mater. 57 (2003) 297–308.
[11] G.A. Peterson, R.J. Schmidt, Handbook of Petroleum Refining Processes, 2004.
[12] C. Perego, R. Millini, W.O. Parker Jr, G. Bellussi, U. Romano, M.C.a.L.H.C.E. van Steen, Studies in Surface Science and Catalysis, Elsevier, 2004.
[13] C. Perego, S. Amarilli, R. Millini, G. Bellussi, G. Girotti, G. Terzoni, Microporous Mater. 6 (1996) 395–404.
[14] M. Tromp, J.A. van Bokhoven, M.T. Garriga Oostenbrink, J.H. Bitter, K.P. de Jong, D.C. Koningsberger, J. Catal. 190 (2000) 209–214.
[15] B.O. Hincapie, L.J. Garces, Q. Zhang, A. Sacco, S.L. Suib, Microporous Mesoporous Mater. 67 (2004) 19–26.
[16] S. van Donk, J.H. Bitter, A. Verberckmoes, M. Versluijs-Helder, A. Broersma, K.P. de Jong, Angew. Chem., Int. Ed. 44 (2005) 1360–1363.
[17] M. Boveri, C. Marquez-Alvarez, M.A. Laborde, E. Sastre, Catal. Today 114 (2006) 217–225.
[18] K.-H. Chung, Microporous Mesoporous Mater. 111 (2008) 544–550.
[19] L.D. Fernandes, P.E. Bartl, J.F. Monteiro, J.G. da Silva, S.C. de Menezes, M.J.B. Cardoso, Zeolites 14 (1994) 533–540.
[20] A.W. O'Donovan, C.T. O'Connor, K.R. Koch, Microporous Mater. 5 (1995) 185–202.
[21] R. Giudici, H.W. Kouwenhoven, R. Prins, Appl. Catal., A 203 (2000) 101–110.
[22] B.L. Meyers, T.H. Fleisch, G.J. Ray, J.T. Miller, J.B. Hall, J. Catal. 110 (1988) 82–95.
[23] M.M. Olken, J.M. Garces, in: R. van Ballmoos (Ed.), 9th IZC, Butterworth-Heinemann, Montreal, 1992, pp. 559–566.
[24] J.M. Garcés, M.M. Olken, G.J. Lee, G.R. Meima, P.A. Jacobs, J.A. Martens, Top. Catal. 52 (2009) 1175–1181.
[25] G.S.J. Lee, J.M. Garces, G.R. Meima, M.J.M. Van Der Aalst, US Patent 5 198 595, The Dow Chemical Company, 1993.
[26] S. van Donk, A. Broersma, O.L.J. Gijzeman, J.H. Bitter, K.P. de Jong, Stud. Surf. Sci. Catal., Elsevier, 2001, pp. 269–269.
[27] A.J. Koster, U. Ziese, A.J. Verkleij, A.H. Janssen, K.P. de Jong, J. Phys. Chem. B 104 (2000) 9368–9370.
[28] M. Ogura, S. Shinomiya, J. Tateno, Y. Nara, E. Kikuchi, M. Matsukata, Chem. Lett. 29 (2000) 882.
[29] M. Ogura, S. Shinomiya, J. Tateno, Y. Nara, M. Nomura, E. Kikuchi, M. Matsukata, Appl. Catal., A 219 (2001) 33–43.
[30] J.C. Groen, J.C. Jansen, J.A. Moulijn, J. Pérez-Ramírez, J. Phys. Chem. B 108 (2004) 13062–13065.
[31] J.C. Groen, J.A. Moulijn, J. Pérez-Ramírez, Microporous Mesoporous Mater. 87 (2005) 153–161.
[32] J.C. Groen, T. Sano, J.A. Moulijn, J. Pérez-Ramírez, J. Catal. 251 (2007) 21–27.
[33] X. Li, R. Prins, J.A. van Bokhoven, J. Catal. 262 (2009) 257–265.
[34] A.N.C. van Laak, R.W. Gosselink, S.L. Sagala, J.D. Meeldijk, P.E. de Jongh, K.P. de Jong, Appl. Catal., A: Gen. 382 (2010) 65–72.
[35] J.R. Kremer, D.N. Mastronarde, J.R. McIntosh, J. Struct. Biol. 116 (1996) 71–76.
[36] S. Nickell, F. Förster, A. Linaroudis, W.D. Net, F. Beck, R. Hegerl, W. Baumeister, J.M. Plitzko, J. Struct. Biol. 149 (2005) 227–234.
[37] T.W. Ridler, S. Calvard, IEEE T Syst Man Cyb. 8 (1978) 630–632.
[38] G. Bellussi, G. Pazzuconi, C. Perego, G. Girotti, G. Terzoni, J. Catal. 157 (1995) 227–234.
[39] N. Katada, T. Takeguchi, T. Suzuki, T. Fukushima, K. Inagaki, S. Tokunaga, H. Shimada, K. Sato, Y. Oumi, T. Sano, Appl. Catal., A 283 (2005) 63–74.
[40] N. Katada, T. Takeguchi, T. Suzuki, T. Fukushima, K. Inagaki, S. Tokunaga, H. Shimada, K. Sato, Y. Oumi, T. Sano, Appl. Catal., A 283 (2005) 75–84.
[41] M. Müller, G. Harvey, R. Prins, Microporous Mesoporous Mater. 34 (2000) 281–290.
[42] H. Friedrich, P.E. de Jongh, A.J. Verkleij, K.P. de Jong, Chem. Rev. 109 (2009) 1613–1629.
[43] A. Corma, Chem. Rev. 97 (1997) 2373–2420.
[44] S. Ban, A.N.C. van laak, P.E. de Jongh, J.P.J.M. van der Eerden, T.J.H. Vlugt, J. Phys. Chem. C 111 (2007) 17241–17248.
[45] F. Thibault-Starzyk, I. Stan, S. Abelló, A. Bonilla, K. Thomas, C. Fernandez, J.P. Gilson, J. Pérez-Ramírez, J. Catal. 264 (2009) 11–14.
[46] F. Kapteijn, G.B. Marin, J.A. Moulijn, in: R.A. van Santen, P.W.N.M. van Leeuwen, J.A. Moulijn, B.A. Averill (Eds.), Catalysis: An Integrated Approach, second ed., Elsevier, Amsterdam, 1999, pp. 405–406.
[47] M. Guisnet, L. Costa, F.R. Ribeiro, J. Mol. Catal. A: Chem. 305 (2009) 69–83.